

1-25-2008

Modeling of Thermodynamic Properties and Phase Equilibria for the Al-Sm Binary System

Shihuai Zhou

Iowa State University, szhou@ameslab.gov

Ralph E. Napolitano

Iowa State University, ren1@iastate.edu

Follow this and additional works at: http://lib.dr.iastate.edu/mse_pubs



Part of the [Metallurgy Commons](#)

The complete bibliographic information for this item can be found at http://lib.dr.iastate.edu/mse_pubs/168. For information on how to cite this item, please visit <http://lib.dr.iastate.edu/howtocite.html>.

This Article is brought to you for free and open access by the Materials Science and Engineering at Iowa State University Digital Repository. It has been accepted for inclusion in Materials Science and Engineering Publications by an authorized administrator of Iowa State University Digital Repository. For more information, please contact digirep@iastate.edu.

Modeling of Thermodynamic Properties and Phase Equilibria for the Al-Sm Binary System

Abstract

The thermodynamic properties and associated phase equilibria for the Al-Sm binary system are examined, and experimental results regarding the stability of the Al₃Sm, Al₁₁Sm₃, and Al₄Sm intermetallics are incorporated. In the analysis presented, the liquid phase is described using a three-species association model, the intermediate phases are treated as stoichiometric compounds, and the terminal phases are treated as solid solutions with a single sublattice model. In addition to the stable phases, thermodynamic descriptions of the metastable Al₁₁Sm₃-*a* and Al₄Sm-*γ* phases are employed, and both stable and metastable phase equilibria are presented over the full composition range, providing a general model, which is consistent with available experimental data. Metastable liquidus curves are examined with respect to the observed crystallization behavior of amorphous Al-Sm alloys.

Keywords

Ames Laboratory, Materials and Engineering Physics

Disciplines

Metallurgy

Comments

This article is from *Metallurgical and Materials Transactions A* 39 (2008): 502, doi:10.1007/s11661-007-9445-6. Posted with permission.

Rights

Copyright 2008 ASM International. This paper was published in *Metallurgical and Materials Transactions A*, Vol. 39, Issue 3, pp. 502-512 and is made available as an electronic reprint with the permission of ASM International. One print or electronic copy may be made for personal use only. Systematic or multiple reproduction, distribution to multiple locations via electronic or other means, duplications of any material in this paper for a fee or for commercial purposes, or modification of the content of this paper are prohibited.

Modeling of Thermodynamic Properties and Phase Equilibria for the Al-Sm Binary System

S.H. ZHOU and R.E. NAPOLITANO

The thermodynamic properties and associated phase equilibria for the Al-Sm binary system are examined, and experimental results regarding the stability of the Al_3Sm , $\text{Al}_{11}\text{Sm}_3$, and Al_4Sm intermetallics are incorporated. In the analysis presented, the liquid phase is described using a three-species association model, the intermediate phases are treated as stoichiometric compounds, and the terminal phases are treated as solid solutions with a single sublattice model. In addition to the stable phases, thermodynamic descriptions of the metastable $\text{Al}_{11}\text{Sm}_3\text{-}\alpha$ and $\text{Al}_4\text{Sm-}\gamma$ phases are employed, and both stable and metastable phase equilibria are presented over the full composition range, providing a general model, which is consistent with available experimental data. Metastable liquidus curves are examined with respect to the observed crystallization behavior of amorphous Al-Sm alloys.

DOI: 10.1007/s11661-007-9445-6

© The Minerals, Metals & Materials Society and ASM International 2008

I. INTRODUCTION

THE formation of crystalline phases in aluminum rare-earth (Al-RE) binary alloys has received considerable attention due to a number of interesting phenomena related to rapid solidification,^[1] glass formation,^[2-5] devitrification behavior,^[6] nanocrystalline applications,^[7,8] and metastable phase transformations.^[9-11] By virtue of these features, it is clear that the binary Al-Sm system is one in which the metastable phases play a major role in the various solidification and devitrification phenomena. As such, accurate thermodynamic treatments of equilibrium and metastable phases are required to use this system as a model for the investigation of fundamental competition and selection principles in systems far from equilibrium.

Considerable work has been done to quantify the various phase equilibria in the Al-Sm system,^[12-20] and the reader is referred to our recent review of reported experimental and modeling efforts.^[11] In addition, the reader is referred to Table I of Reference 11 for a comprehensive summary of the structure and composition of the various stable and metastable phases observed in the Al-Sm binary system.

The most current Al-Sm phase diagram is shown in Figure 1,^[20] and, for the sake of brevity, the inconsistencies that remain unresolved are summarized here. First, prior models^[20] take no account of the metastable γ phase (orthorhombic, Al_4U type), which has been

observed in various devitrification sequences.^[9,10] We have previously investigated the relative stability of the γ phase along with other Al_4Sm and $\text{Al}_{11}\text{Sm}_3$ phases and incorporate our prior results into the general model here.^[11] Second, while experimental evidence for the relative stability of the α phase is unclear,^[12-20] it has been treated as a stable phase, and it appears in the equilibrium phase diagram proposed by Saccone,^[20] as shown in Figure 1. Our prior work, however, suggests that α has no range of full stability but rather that it is metastable down to 0 K,^[11] which is reflected in the current treatment. Third, reported experimental data for the region between the $L \rightarrow \beta + \sigma$ and $\beta + \sigma \rightarrow \delta$ reactions are not sufficient to clearly establish the associated phase equilibria, as indicated in Figure 1. Specifically, calorimetry measurements^[14,15,20] suggest that there may be an invariant near 1490 K, between the $L \rightarrow \beta + \sigma$ and $\beta + \sigma \rightarrow \delta$ reactions. This feature would be similar to that observed in the Al-La system, which exhibits a stable Al_7La_3 phase in this temperature range. Moreover, inconsistent reports of the $L \rightarrow \beta + \sigma$ eutectic invariant^[14,15,20] and poor agreement between prior models^[20] and experimental data^[14,15,20] (Table I) indicate that better thermodynamic descriptions of the liquid phase are necessary.

In this article, each of these issues is addressed through the development of a general model for the thermodynamic properties of the Al-Sm system. Experimental measurements are included to clarify the stability of the Al_7Sm_3 compound, and an association model, capable of describing the chemical short-range order in the liquid phase, is employed. In addition, our formulation includes thermodynamic descriptions of the metastable $\text{Al}_{11}\text{Sm}_3\text{-}\alpha$ and $\text{Al}_4\text{Sm-}\gamma$ phases. The model parameters, describing the Gibbs free energies associated with the formation of compounds or solution phases, are determined through a systematic semiempirical optimization, employing experimental data from current work and those available in the

S.H. ZHOU, Assistant Scientist, is with Materials and Engineering Physics, Ames Laboratory, USDOE, 204A Wilhelm Hall, Ames, IA 50011. R.E. NAPOLITANO, Associate Professor, Department of Materials Science and Engineering, Iowa State University, 2220 Hoover Hall, Ames, IA 50011, and Scientist with Materials and Engineering Physics, Ames Laboratory, USDOE, 116 Wilhelm Hall, Ames, IA, 50011. Contact e-mail: ralphn@iastate.edu

Manuscript submitted May 23, 2007.

Article published online January 25, 2008

Table I. Invariant Reactions in the Al-Sm Binary System

Reaction	Modeling Results			Experimental Results		
		Present Work	Reference 20	Reference 14	Reference 15	
Liq \rightarrow δ	T, K	1757.6	1747.1	1753	–	1773
	$x_{(liq,Sm)}$	0.333	0.333	0.333	–	0.333
Liq \rightarrow β	$x_{(\delta,Sm)}$	0.333	0.333	0.333	–	0.333
	T, K	1655	1644.9	1653	–	1723
	$x_{(liq,Sm)}$	0.200	0.214	0.200	–	0.205
Liq \rightarrow $\beta + \sigma$	$x_{(\beta,Sm)}$	0.200	0.214	0.200	–	0.205
	T, K	1585.1	1643.5	1613	1473	1501
	$x_{(liq,Sm)}$	0.228	0.222	0.249	–	–
$\beta + \sigma \rightarrow \delta$	$x_{(\beta,Sm)}$	0.200	0.214	0.214	0.200	0.205
	$x_{(\sigma,Sm)}$	0.333	0.333	0.333	0.333	0.333
	T, K	1408.5	1404.3	1403	1378	1407
	$x_{(\beta,Sm)}$	0.200	0.214	0.214	0.200	–
$\beta \rightarrow liq + \delta$	$x_{(\sigma,Sm)}$	0.333	0.333	0.333	0.333	–
	$x_{(\delta,Sm)}$	0.250	0.250	0.25	0.250	–
	T, K	1333.3	1321.3	1343	1328	1351
	$x_{(\beta,Sm)}$	0.200	0.214	0.200	0.200	0.200
Liq + $\sigma \rightarrow \theta$	$x_{(liq,Sm)}$	0.14	0.112	0.130	–	–
	$x_{(\delta,Sm)}$	0.250	0.250	0.250	0.250	–
	T, K	1232.8	1215	1233	–	–
	$x_{(liq,Sm)}$	0.586	0.617	0.578	–	–
Liq + $\theta \rightarrow \chi$	$x_{(\sigma,Sm)}$	0.333	0.333	0.333	–	–
	$x_{(\theta,Sm)}$	0.500	0.500	0.500	–	–
	T, K	1134.7	1121.5	1133	–	–
	$x_{(liq,Sm)}$	0.685	0.670	0.698	–	–
Liq \rightarrow bcc + χ	$x_{(\theta,Sm)}$	0.667	0.500	0.500	–	–
	$x_{(\chi,Sm)}$	0.500	0.667	0.667	–	–
	T, K	1059.0	1039.0	1033	1013	–
	$x_{(liq,Sm)}$	0.833	0.793	0.789	–	–
Bcc \rightarrow rho + χ	$x_{(bcc,Sm)}$	0.940	0.891	0.879	–	–
	$x_{(\chi,Sm)}$	0.667	0.667	0.667	0.667	–
	T, K	974.5	973.6	973	–	–
	$x_{(bcc,Sm)}$	0.957	0.900	~0.9	–	–
Liq \rightarrow fcc + δ	$x_{(rho,Sm)}$	1.000	0.963	0.958	–	–
	$x_{(\chi,Sm)}$	0.667	0.667	0.667	–	–
	T, K	919.5	–	–	903	906
	$x_{(liq,Sm)}$	0.019	–	–	–	–
	$x_{(fcc,Sm)}$	0.00	–	–	0.00	0.00
	$x_{(\delta, Sm)}$	0.250	–	–	0.25	0.25

Invariant Reactions for Metastable Phases

		Present Work	Reference 20	Reference 9	Reference 10
Liq \rightarrow fcc + α	T, K	906.2	897.8*	908	–
	$x_{(liq,Sm)}$	0.034	0.03	~0.03	–
	$x_{(fcc,Sm)}$	0.00	0.00	0.00	–
	$x_{(\alpha,Sm)}$	0.214	0.214	0.214	–
$\beta + \sigma \rightarrow \alpha$	T, K	1361.5	–	–	–
$\beta \rightarrow liq + \alpha$	T, K	1329.4	1321.3*	–	–
$\beta \rightarrow \gamma$	T, K	873	–	–	873

*These are treated as stable phases in Ref. 20.

literature.^[11,14,15,20–33] The resulting thermodynamic properties and the corresponding equilibrium phase diagram are compared with the prior thermodynamic modeling reported by Saccone *et al.*^[20] Finally, the computed metastable liquidus curves for the Al₄Sm- β and fcc phases are examined and compared with reported observations of crystallization from the under-cooled liquid or amorphous state.^[9,10]

II. EXPERIMENTAL MEASUREMENTS

To clarify the phase diagram in the region between the $L \rightarrow \beta + \sigma$ and $\beta + \sigma \rightarrow \delta$ invariants and to resolve the issue of Al₇Sm₃ stability in the high-temperature regime, specimens were heat treated and water quenched to room temperature, varying heat treatment duration and temperature, for alloy compositions between β

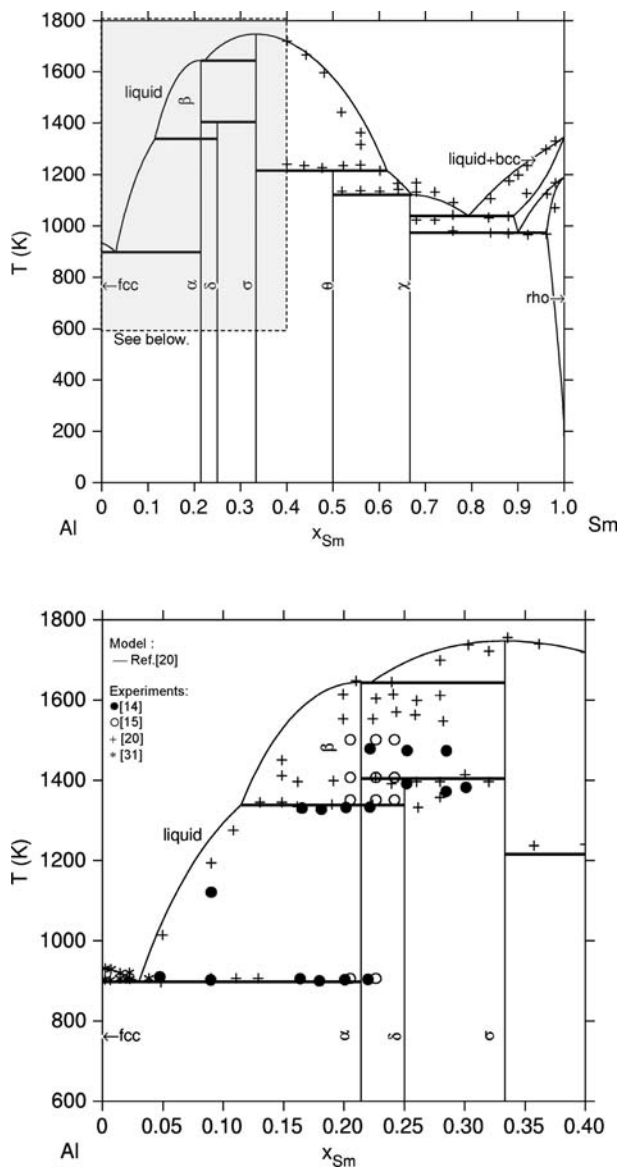


Fig. 1—Previously reported Al-Sm phase diagram,^[20] shown with relevant experimental data, indicating phase transitions determined by calorimetry measurements.^[14,15,20,31]

Table II. EPMA Results Showing the Composition of Observed Phases in Al-30.6 At. Pct Sm after the Indicated Heat Treatment Followed by Water Quenching

Heat Treatment	Phase Compositions, At. Pct Sm		
	σ	δ	β
As cast	30.7	23.1	—
1373 K for 50 h	31.6	24.6	—
1453 K for 15 h	31.3	24.4	21.4
1453 K for 50 h	31.4	—	21.0

(Al₄Sm) and σ (Al₃Sm), as listed in Table II. Alloy test specimens of approximately 15 grams were prepared^[34] by arc melting the pure elements (0.99999 Al and 0.999 Sm, by weight) on a copper hearth in an argon atmosphere. Each alloy specimen was arc-melted three

times to ensure homogeneity and sealed in either quartz (for heating to temperatures below 1453 K) or alumina/tantalum (for heating to temperatures above 1473 K), under an argon atmosphere. Microstructures and phase compositions were characterized using X-ray diffraction (XRD) with Cu K_{α} radiation, scanning electron microscopy (SEM) with energy dispersive spectroscopy (EDS), electron backscatter diffraction (EBSD), and electron probe microanalysis (EPMA) with wavelength dispersive spectroscopy (WDS) (20 kV, ~10 nA).

Microstructure and XRD results from the Al-30.6 at. pct Sm test alloy heat treated at 1453 K are summarized in Figures 2 through 5. Typical microstructures observed after heat treatments of 0, 15, and 50 hours (0, 5.4×10^4 , and 1.8×10^5 s, respectively) are shown in Figure 2. The pictured sequence reveals a two-phase structure in the as-cast alloy, which passes through a

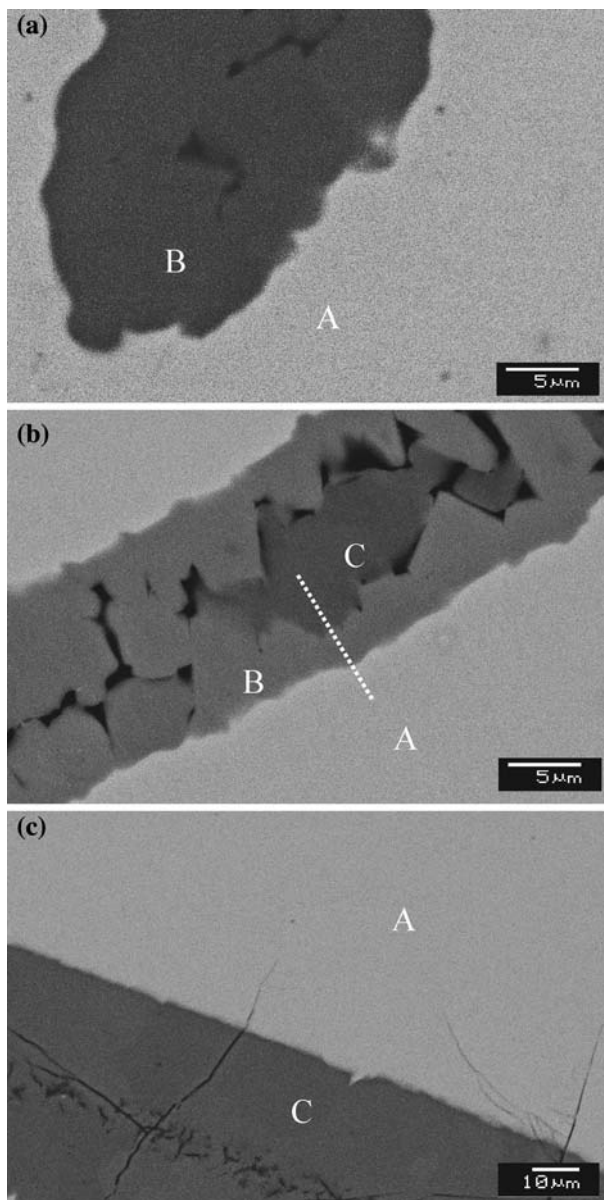


Fig. 2—SEM images showing observed microstructures for Al-30.6 at. pct Sm: (a) as cast, (b) 15 h at 1453 K, and (c) 50 h at 1453 K.

three-phase intermediate state and ultimately evolves into a two-phase structure that is different from the initial as-cast state during heat treatment. Corresponding XRD patterns are shown in Figure 3. The diffraction data in Figure 3(a) indicate the presence of the σ and δ phases in the as-cast (0 hour) specimen. Figure 2(b) shows that a third phase appears after 15 hours at 1453 K (location C), but due to its small volume fraction, it cannot be identified from the XRD data shown Figure 3(b). The EPMA composition measurements in Table II, however, suggest that the third phase in Figure 2(b) is β (Al_4Sm). Indeed, the three phases in the intermediate state are clearly distinguishable on the basis of composition, as shown by the profile in Figure 4, which was measured along the dashed line in Figure 2(b). Finally, well-indexed EBSD patterns clearly support the identification of these three phases, as shown in the orientation maps in Figure 5, where locations A, B, and C in Figure 3 are associated with σ , δ , and β , respectively.

With confirmation of the phase identities, the image sequence in Figure 2 reveals that the microstructure evolves during heat treatment from $\sigma + \delta$ at 0 hours

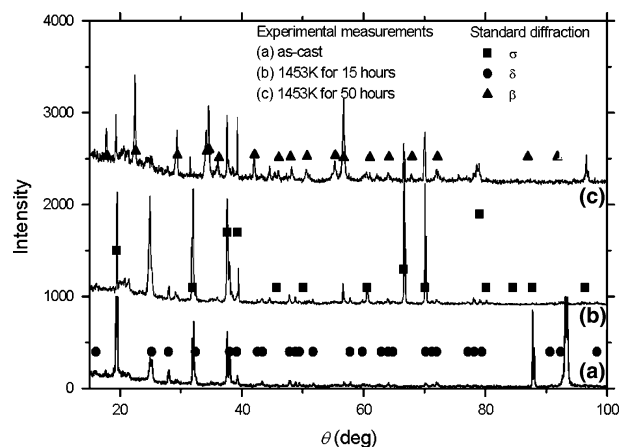


Fig. 3—XRD data for both as-cast and heat-treated (at 1453 K) alloys.

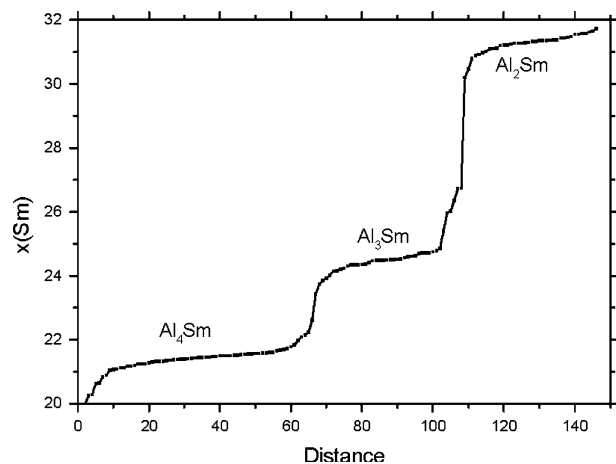


Fig. 4—Composition profile along the dashed line in Fig. 2(b), measured using EPMA.

(as cast) to $\sigma + \delta + \beta$ after 15 hours, and finally to $\sigma + \beta$ after 50 hours at 1453 K. Thus, it is concluded that β and σ (but not Al_7Sm_3) are in equilibrium at 1453 K. Similar analysis after a 50-hour heat treatment indicates that the $\sigma + \delta$ two-phase combination is stable at 1373 K. These results suggest that the $\beta + \sigma \rightarrow \delta$ peritectoid invariant must lie between 1373 and 1453 K, which is consistent with prior experimental reports.^[14,15,20] A number of additional heat treatments, intended to clarify the ($L \rightarrow \beta + \sigma$) eutectic temperature, were performed but were inconclusive due to the evaporation of Sm at higher temperatures.*

*Heat treatments of 60 to 80 h at 1508 and 1543 K produced a considerable amount of Sm evaporation, with a distinct film of Sm deposited on the crucible walls. Similar observations were reported by Buschow and Vucht.^[14] Inconsistencies in reported values for the $L \rightarrow \beta + \sigma$ eutectic temperature^[14,15,20] may be due to such experimental difficulties.

III. THERMODYNAMIC MODELING

The phase equilibria in the Al-Sm binary system are described here by modeling the Gibbs free energy for each relevant phase over the appropriate range of composition at constant pressure (1 atm). The thermodynamic properties of pure Al and Sm in various structures are computed using the parameters^[35] listed in Table III. The thermodynamics of the binary Al-Sm system are described using a chemical associate approach for the liquid phase and simple binary substitutional solution models for the fcc, bcc, and rho phases. The intermediate phases are treated as stoichiometric compounds. All thermodynamic models are defined in Table IV, where the total Gibbs free energy for any phase, Φ , is given by the sum of three contributions:

$$G_m^\Phi = {}^{\text{ref}}G_m^\Phi + {}^{\text{id}}G_m^\Phi + {}^{\text{xs}}G_m^\Phi \quad [1]$$

where the subscript m denotes that all terms are molar quantities. The first term in Eq. [1] is given by the sum of occupancy-weighted sublattice end-member contributions. The second and third terms are the ideal and excess parts of the Gibbs free energy of mixing, respectively. As shown in Table IV, a Redlich-Kister polynomial^[36] is used to describe the composition and temperature dependence of the excess mixing contribution for the solid solution phases. The specific formulation of the Gibbs free energy for each phase is described in Section A.

A. Model Formulation

The fcc, bcc, and rho phases are treated as simple binary substitutional solutions with Gibbs free energies described as listed in Table IV, where x_i denotes the mole fraction of component i , and ${}^\circ G_i^\Phi$ ($i = \text{Al}, \text{Sm}$) denotes the molar Gibbs free energy of the pure element i with the structure Φ ($\Phi = \text{fcc}, \text{bcc}, \text{and rho}$). Also, ${}^{\text{xs}}G_m^\Phi$ is the excess Gibbs free energy expressed with the interaction parameters ${}^j L_{\text{Al,Sm}}^\Phi$ to be evaluated primarily on the basis of experimental data. Here, the fcc and rho phases are treated as ideal solutions, and the $j = 0$ and

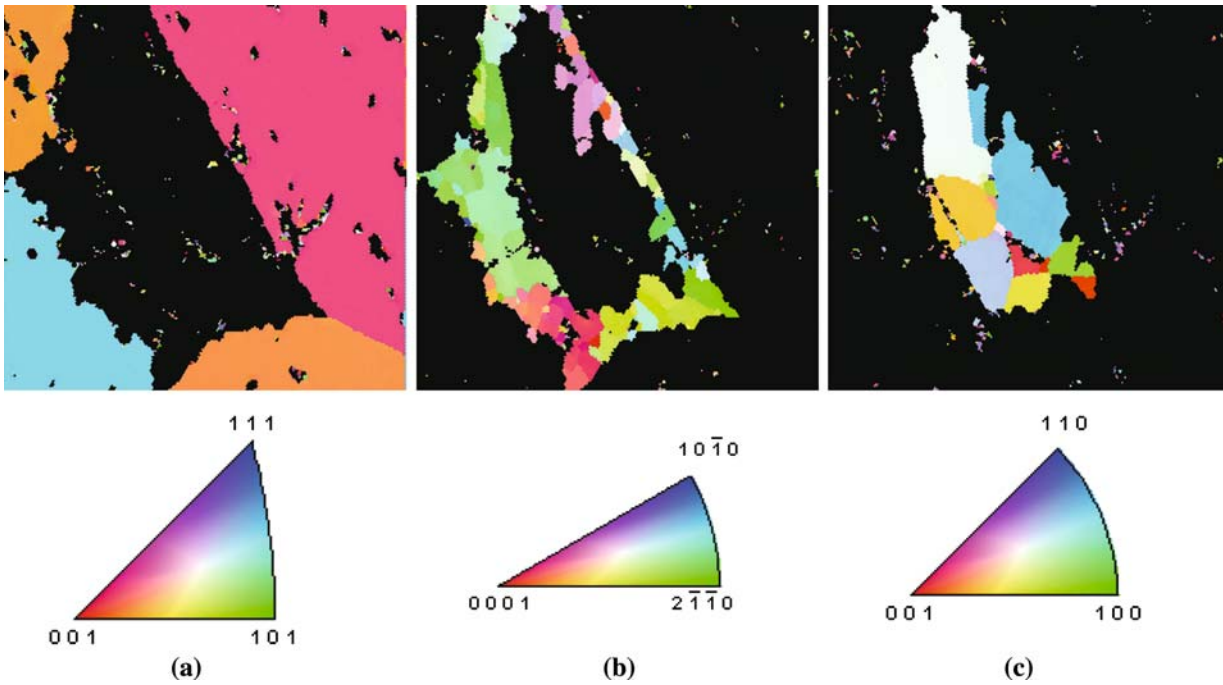


Fig. 5—EBSD maps showing a microstructure of indexed orientations for three distinct phases in a Al-30.6 at. pct Sm specimen, heat treated at 1453 K for 15 h. (a) $\text{Al}_2\text{Sm}-\sigma$, (b) $\text{Al}_3\text{Sm}-\delta$, and (c) $\text{Al}_4\text{Sm}-\beta$.

$j = 1$ terms for the bcc phase are computed by treating ${}^0L_{\text{Al,Sm}}^{\text{bcc}}$ and ${}^1L_{\text{Al,Sm}}^{\text{bcc}}$ as constants. The intermediate phases are assumed to be stoichiometric compounds of the form Al_pSm_q , each with a Gibbs free energy given in Table IV, where $\Delta G_{\text{Al}_p\text{Sm}_q}^\circ$ is the Gibbs free energy of formation of the compound Al_pSm_q from the pure component ground states.

The Gibbs free energy of the liquid phase is given by

$$G_m^{\text{liq}} = x_{\text{Al}} {}^\circ G_{\text{Al}}^{\text{liq}} + x_{\text{Sm}} {}^\circ G_{\text{Sm}}^{\text{liq}} + \Delta G_m^{\text{liq}} \quad [2]$$

where ${}^\circ G_i^{\text{liq}}$ is the Gibbs free energy of the indicated component. To model the mixing contribution, ΔG_m^{liq} , a three-species association model^[37,38] is employed, where the Al_2Sm composition is chosen as the relevant intermediate chemical associate due to its melting temperature maximum. Thus, the liquid is considered to be a solution of Al, Sm, and Al_2Sm associates, containing m_{Al} , m_{Sm} , and $m_{\text{Al}_2\text{Sm}}$ moles of each, respectively, with the total number of moles of associates given by

$$m = m_{\text{Al}} + m_{\text{Sm}} + m_{\text{Al}_2\text{Sm}} \quad [3]$$

and the corresponding associate mole fractions given by

$$y_i = m_i/m \quad [4]$$

Recognizing that the system remains constrained by the conservation of elemental components (*i.e.*, $n = n_{\text{Al}} + n_{\text{Sm}}$) and that the associate mole numbers are related to the component mole numbers as

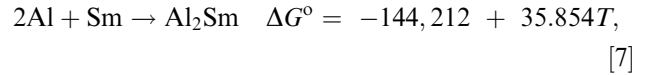
$$n_{\text{Al}} = m_{\text{Al}} + 2m_{\text{Al}_2\text{Sm}}$$

$$n_{\text{Sm}} = m_{\text{Sm}} + m_{\text{Al}_2\text{Sm}}, \quad [5]$$

we note further that

$$n = m_{\text{Al}} + m_{\text{Sm}} + 3m_{\text{Al}_2\text{Sm}}. \quad [6]$$

Considering now the associate formation reaction and its standard Gibbs free energy change (Table V),



the equilibrium extent of the association reaction (*i.e.*, the equilibrium associate mole fractions) is computed as

$$\frac{y_{\text{Al}_2\text{Sm}}}{y_{\text{Al}}^2 y_{\text{Sm}}} = \frac{\gamma_{\text{Al}}^2 \gamma_{\text{Sm}}}{\gamma_{\text{Al}_2\text{Sm}}} \exp\left(-\frac{\Delta G_{\text{Al}_2\text{Sm}}^\circ}{RT}\right), \quad [8]$$

where γ_i are the activity coefficients for the associate mixture, and $\Delta G_{\text{Al}_2\text{Sm}}^\circ$ is the standard Gibbs free energy of formation for the associate (Eq. [7]). The total enthalpy and entropy of mixing for the system are thus modeled as

$$\Delta H^{\text{liq}} = m(y_{\text{Al}} y_{\text{Sm}} {}^0L_{\text{Al,Sm}}^{\text{liq}} + y_{\text{Al}} y_{\text{Al}_2\text{Sm}} {}^0L_{\text{Al,Al}_2\text{Sm}}^{\text{liq}} + y_{\text{Al}_2\text{Sm}} y_{\text{Sm}} {}^0L_{\text{Al}_2\text{Sm,Sm}}^{\text{liq}}) + m_{\text{Al}_2\text{Sm}} \Delta H_{\text{Al}_2\text{Sm}}^\circ \quad [9a]$$

$$\Delta S^{\text{liq}} = mR(y_{\text{Al}} \ln y_{\text{Al}} + y_{\text{Al}_2\text{Sm}} \ln y_{\text{Al}_2\text{Sm}} + y_{\text{Sm}} \ln y_{\text{Sm}}) + m_{\text{Al}_2\text{Sm}} \Delta S_{\text{Al}_2\text{Sm}}^\circ, \quad [9b]$$

where the ${}^0L_{i,j}^{\text{liq}}$ interaction parameters are assumed to be constant and are evaluated with experimental data. From Eq. [9], the molar enthalpy and entropy of mixing for the system are computed as

Table III. Coefficients for the Standard Gibbs Free Energies of Pure Al and Sm in the Relevant Phases^[35]

Parameter (Liquid Phase)		${}^{\circ}G_{\text{Al}}^{\text{L}}$		${}^{\circ}G_{\text{Sm}}^{\text{L}}$	
T_{min}	298	933.47	298	1190	
T_{max}	933.47	3200	1190	2100	
${}^{\circ}G_{\text{Al}}^{\text{ref}}$	—	—	—	—	—
a_0	11005.03	-795.996	3468.783	-11728.229	
a_1	-11.841867	177.430178	20.117456	273.48707	
a_2	—	-31.748192	-11.696828	-50.208	
a_3	—	—	-0.032418177	—	
a_4	—	—	4.54427×10^{-6}	—	
a_5	—	—	—	—	
a_6	—	—	23,528	—	
a_7	—	—	—	—	
a_8	7.9337×10^{-20}	—	—	—	
(Fcc Phase)		${}^{\circ}G_{\text{Al}}^{\text{fcc}}$			
T_{min}	298	700	933.47	—	
T_{max}	700	933.47	2900	—	
${}^{\circ}G_{\text{Al}}^{\text{ref}}$	—	—	—	—	—
a_0	7976.15	-11276.24	-11278.37	—	
a_1	137.093038	223.048446	188.68415	—	
a_2	-24.3671976	-38.5844296	-31.74819	—	
a_3	-0.001884662	0.018531982	—	—	
a_4	-8.77664×10^{-7}	-5.76422×10^{-6}	—	—	
a_5	—	—	—	—	
a_6	74092	74092	—	—	
a_7	—	—	-1.2305×10^{28}	—	
a_8	—	—	—	—	
(Bcc Phase)		${}^{\circ}G_{\text{Al}}^{\text{bcc}}$		${}^{\circ}G_{\text{Sm}}^{\text{bcc}}$	
T_{min}	298	298	1190	1345	
T_{max}	3200	1190	1345	2100	
${}^{\circ}G_{\text{Al}}^{\text{ref}}$	—	—	—	—	—
a_0	10,083	-4368.72	-15957.862	111191.653	
a_1	-4.813	55.972523	253.121044	-624.680805	
a_2	—	-16.929849	-46.9445	71.6856914	
a_3	—	-0.02544601	—	-0.004731496	
a_4	—	3.5795×10^{-6}	—	3.32986×10^{-6}	
a_5	—	—	—	—	
a_6	—	94209	—	-24870276	
a_7	—	—	—	—	
a_8	—	—	—	—	
(Rho Phase)		${}^{\circ}G_{\text{Sm}}^{\text{rho}}$			
T_{min}	298	700	1190	1345	
T_{max}	700	1190	1345	2100	
${}^{\circ}G_{\text{Al}}^{\text{ref}}$	—	—	—	—	—
a_0	-3872.013	-50078.215	289719.819	-23056.079	
a_1	-32.10748	627.869894	-2744.50976	282.194375	
a_2	-1.6485	-102.665	381.41982	-50.208	
a_3	-0.050254	0.0474522	-0.254986338	—	
a_4	1.01035×10^{-5}	-7.5384×10^{-6}	2.751215×10^{-5}	—	
a_5	—	—	—	—	
a_6	-82168	3861770	-40102102	—	
a_7	—	—	—	—	
a_8	—	—	—	—	

Note: ${}^{\circ}G = {}^{\circ}G^{\text{ref}} + a_0 + a_1T + a_2T \ln T + a_3T^2 + a_4T^3 + a_5T^4 + a_6T^{-1} + a_7T^{-9} + a_8T^7$ (J/mol) with $T_{\text{min}} < T < T_{\text{max}}$.

Table IV. Summary of the Thermodynamic Models Used for the Al-Sm Binary System

Phase	Prototype	Method (Formulation)	Model
Liquid	–	association model (Al,Al ₂ Sm,Sm)	See Eq. [10]
Fcc-Al	Cu	one-sublattice model (Al,Sm) [†]	${}^{\text{ref}}G_m^\phi = \sum_{i=\text{Al,Sm}} x_i^\circ G_i^\phi$
Bcc-Sm	W		${}^{\text{id}}G_m^\phi = RT \sum_{i=\text{Al,Sm}} x_i \ln x_i$
Rho-Sm	α -Sm		${}^{\text{xs}}G_m^\phi = x_{\text{Al}}x_{\text{Sm}} \sum_{j=0}^n {}^jL_{\text{Al,Sm}}^\phi (x_{\text{Al}} - x_{\text{Sm}})^j$
α -Al ₁₁ Sm ₃	Al ₁₁ La ₃ - α	(Al) _{0.8} (Sm) _{0.2}	$G_m^\phi = \Delta G_{\text{Al}_p\text{Sm}_q}^\phi + p^\circ G_{\text{Al}}^{\text{fcc}} + q^\circ G_{\text{Sm}}^{\text{rho}}$ $= a^\phi + b^\phi T + p^\circ G_{\text{Al}}^{\text{fcc}} + q^\circ G_{\text{Sm}}^{\text{rho}}$
β -Al ₄ Sm	Al ₄ Ba	(Al) _{0.8} (Sm) _{0.2}	
δ -Al ₃ Sm	Ni ₃ Sn	(Al) _{0.75} (Sm) _{0.25}	
σ -Al ₂ Sm	Cu ₂ Mg	(Al) _{0.67} (Sm) _{0.33}	
θ -AlSm	AlEr	(Al) _{0.5} (Sm) _{0.5}	
χ -AlSm ₂	Co ₂ Si	(Al) _{0.33} (Sm) _{0.67}	
γ -Al ₄ Sm	Al ₄ U	(Al) _{0.8} (Sm) _{0.2}	

Table V. Evaluated Thermodynamic Model Parameters

Phase	Parameter	Value (J/mol)
Liquid	${}^0L_{\text{Al,Sm}}^{\text{liq}}$	-80524
	${}^0L_{\text{Al,Al}_2\text{Sm}_1}^{\text{liq}}$	-26012
	${}^0L_{\text{Al}_2\text{Sm}_1,\text{Sm}}^{\text{liq}}$	-42022
	$\Delta G_{\text{Al}_2\text{Sm}_1}^\circ$	-144212 + 35.854T
Bcc	${}^0L_{\text{Al,Sm}}^{\text{bcc}}$	-57431
	${}^1L_{\text{Al,Sm}}^{\text{bcc}}$	18102
Al ₄ Sm- β	$\Delta G_{\text{Al:Sm}}^\beta$	-23121 - 6.202T
Al ₁₁ Sm ₃ - α	$\Delta G_{\text{Al:Sm}}^\alpha$	-34800 + 1.344T
Al ₄ Sm- γ	$\Delta G_{\text{Al:Sm}}^\gamma$	-28535
Al ₃ Sm- δ	$\Delta G_{\text{Al:Sm}}^\delta$	-48386 + 8.342T
Al ₂ Sm- σ	$\Delta G_{\text{Al:Sm}}^\sigma$	-55000 + 7.382T
AlSm- θ	$\Delta G_{\text{Al:Sm}}^\theta$	-49000 + 9.446T
AlSm ₂ - χ	$\Delta G_{\text{Al:Sm}}^\chi$	-37300 + 8.799T

Note: Compound prototypes and structures are given in Table I of Ref. [11].

$$\Delta H_m^{\text{liq}} = \frac{m}{n} \left(y_{\text{Al}} y_{\text{Sm}} {}^0L_{\text{Al,Sm}}^{\text{liq}} + y_{\text{Al}} y_{\text{Al}_2\text{Sm}} {}^0L_{\text{Al,Al}_2\text{Sm}}^{\text{liq}} + y_{\text{Al}_2\text{Sm}} y_{\text{Sm}} {}^0L_{\text{Al}_2\text{Sm},\text{Sm}}^{\text{liq}} + y_{\text{Al}_2\text{Sm}} \Delta H_{\text{Al}_2\text{Sm}}^\circ \right) \quad [10a]$$

$$\Delta S_m^{\text{liq}} = \frac{m}{n} R \left(y_{\text{Al}} \ln y_{\text{Al}} + y_{\text{Al}_2\text{Sm}} \ln y_{\text{Al}_2\text{Sm}} + y_{\text{Sm}} \ln y_{\text{Sm}} + y_{\text{Al}_2\text{Sm}} \Delta S_{\text{Al}_2\text{Sm}}^\circ \right). \quad [10b]$$

Here, the five parameters (${}^0L_{\text{Al,Sm}}^{\text{liq}}$, ${}^0L_{\text{Al,Al}_2\text{Sm}}^{\text{liq}}$, ${}^0L_{\text{Al}_2\text{Sm},\text{Sm}}^{\text{liq}}$, $\Delta H_{\text{Al}_2\text{Sm}}^\circ$, $\Delta S_{\text{Al}_2\text{Sm}}^\circ$) are left for evaluation from experimental data, as listed in Table V. Finally, from Eqs. [4–6], the ratio of mole numbers is given by

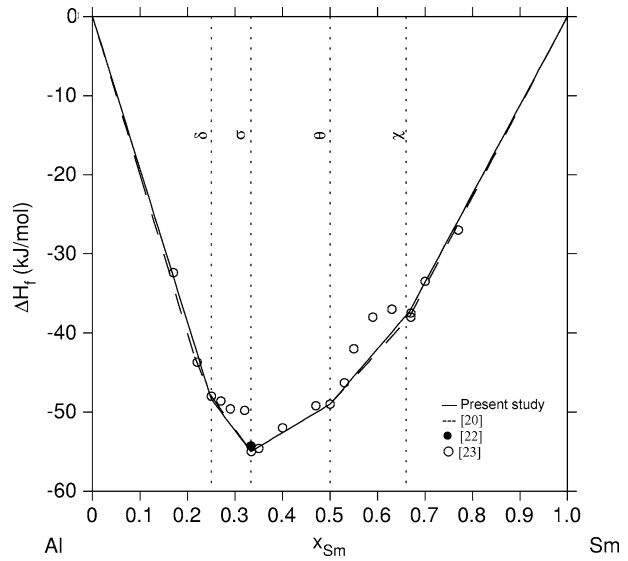


Fig. 6—Enthalpy of formation for 298 K, calculated using the parameters in Table V.

$$\frac{n}{m} = 1 + 2y_{A_2B} \quad [11]$$

and therefore varies with the extent of the association reaction (Eq. [7]) dictated by the standard Gibbs free energy change, as in Eq. [8]. The temperature dependence of the equilibrium associate fractions in the Al-Sm liquid, according to our model, will be discussed in a subsequent section C. Note: Compound prototypes and structures are given in Table I of Ref. [11].

B. Determination of Thermodynamic Model Parameters

In the thermodynamic models described in the preceding section, we establish eight Gibbs free energy of formation parameters and five interaction (*i.e.*, mixing) parameters, as listed in Table V. The following discussion details our evaluation of these thermodynamic model parameters.

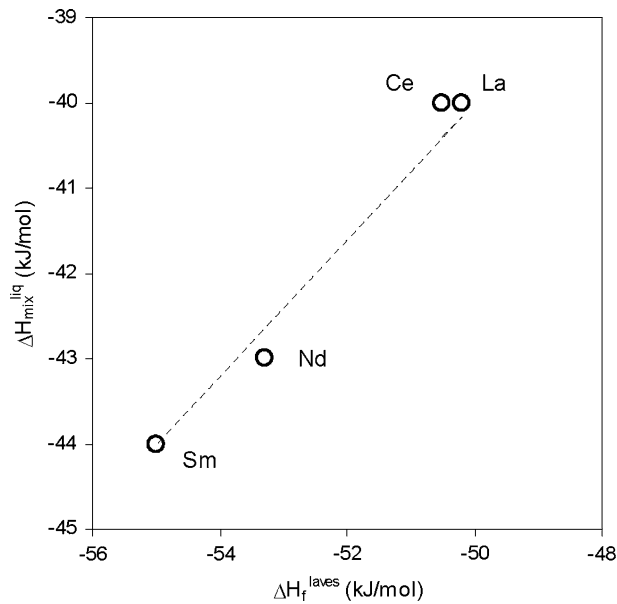


Fig. 7—Enthalpy of mixing for Al-RE (RE = La, Ce, Nd, and Sm) liquids vs reported enthalpy of formation for the corresponding Al₂RE compounds.^[21,22,24–29,32,33,39] The estimated value for liquid Al₂Sm is also shown.

Colinet *et al.*^[22] and Borzone *et al.*^[23] have measured the enthalpy of formation at 298 K in Al-Sm as a function of composition, as shown in Figure 6. These data are employed here to evaluate the parameters a^ϕ (Table IV) for each of the intermetallic phases that are stable at room temperature. There are currently no such data available for the liquid phase. To estimate the enthalpy of mixing for the liquid, several similar systems of lanthanide alloys of aluminum are considered here, specifically Al-La,^[21,22,24–27,39] Al-Ce,^[22,28,29,32] and Al-Nd.^[22,33] For these three binary systems, the enthalpy of mixing for the liquid is compared to the enthalpy of formation for the laves phase (*i.e.*, Cu₂Mg-type), and it is noted that (for $x_{\text{Sm}} = 0.333$) the ratio, $\Delta H_{\text{mixing}}^{\text{liq}} / \Delta H_{\text{formation}}^{\text{Al}_2\text{Ln}}$, is roughly constant and approximately equal to 4/5, as shown in Figure 7. Assuming then a similar ratio for the Al-Sm system and using the reported value of $\Delta H_{\text{formation}}^{\text{Al}_2\text{Sm}} = -55$ kJ/mol,^[22,23] the value of $\Delta H_{\text{mixing}}^{\text{liq}}$ is estimated to be -44 kJ/mol. Finally, phase equilibrium data^[14,20] are used to evaluate the remaining parameters simultaneously, as listed in Table V.

In addition to the stable phases, the metastable phases Al₁₁Sm₃- α and Al₄Sm- γ are included in our model. For the Al₁₁Sm₃- α phase, the parameter a^α is determined from our previous first-principles calculation results.^[11] For b^α , we note that the temperature for the metastable $\beta \rightarrow \alpha + L$ decomposition reaction must be below the stable $\beta \rightarrow \delta + L$ invariant temperature of 1333.3 K (Table I). Reported experimental data indicate that the $\beta \rightarrow \alpha + L$ reaction occurs between 1328 and 1351 K.^[14,15,20] Here the lower limit of the indicated range is selected, and it is assumed that the $\beta \rightarrow \alpha + L$ invariant temperature is 1328 K. With this temperature,

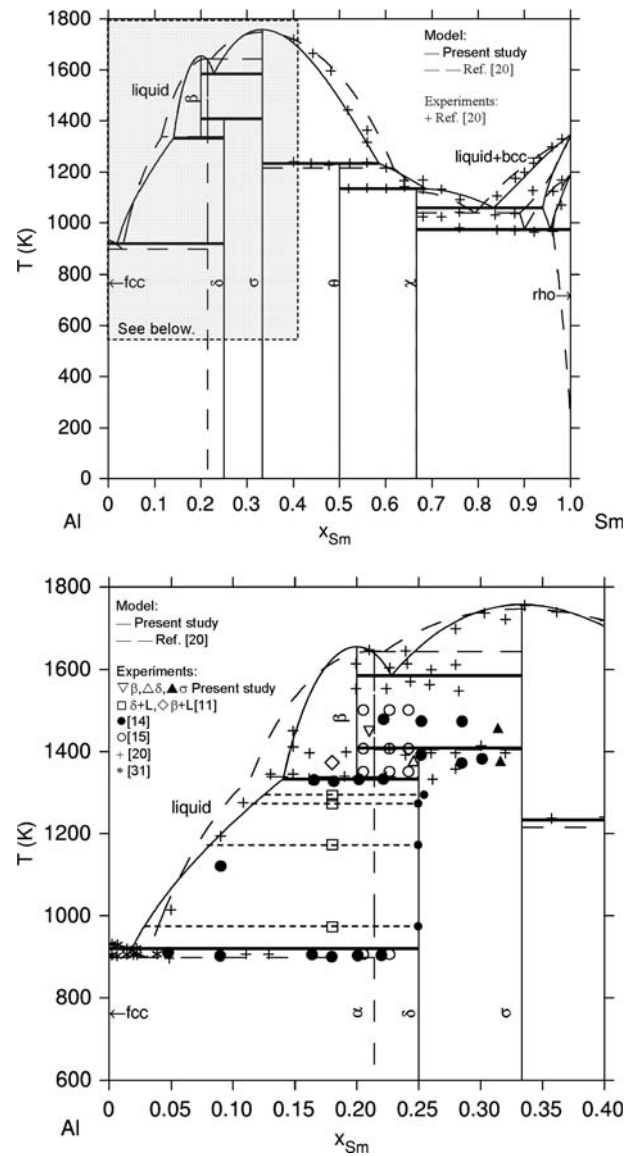


Fig. 8—Al-Sm phase diagram resulting from the present model (*i.e.*, computed using the parameters listed in Tables III and IV), compared with the model of Ref. 20 and relevant experimental data (Fig. 1). The tie-lines for the open squares denote $L + \delta$ equilibrium with the indicated δ phase compositions.^[11]

the parameter b^α is evaluated as listed in Table V. For the Al₄Sm- γ phase, it is assumed that $b^\gamma = 0$, and a^γ is evaluated from the reported $\beta \rightarrow \gamma$ transition temperature of 873 K^[9,10] (Table V).

C. Phase Equilibria and Thermodynamic Properties

The Al-Sm phase diagram computed from the Gibbs free energy functions for the involved phases, employing the model formulation and parameter assessment described above, is shown in Figure 8. Relevant experimental data^[11,14,15,20,31] as well as the phase diagram proposed by Saccone *et al.*^[20] are also shown for comparison. The treatment proposed here includes two

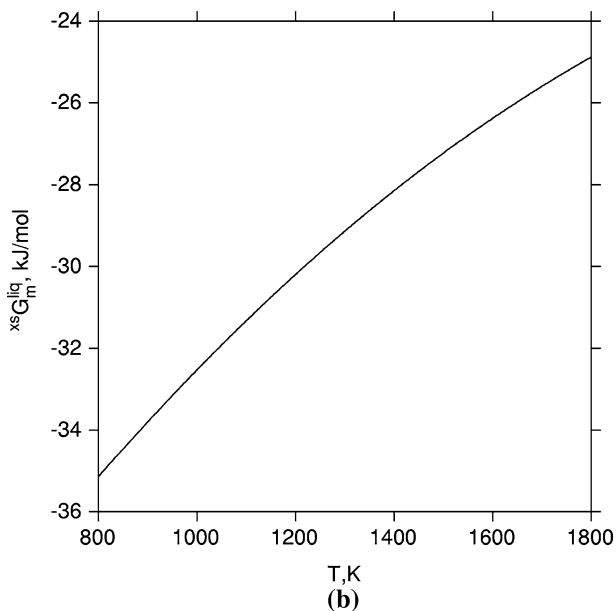
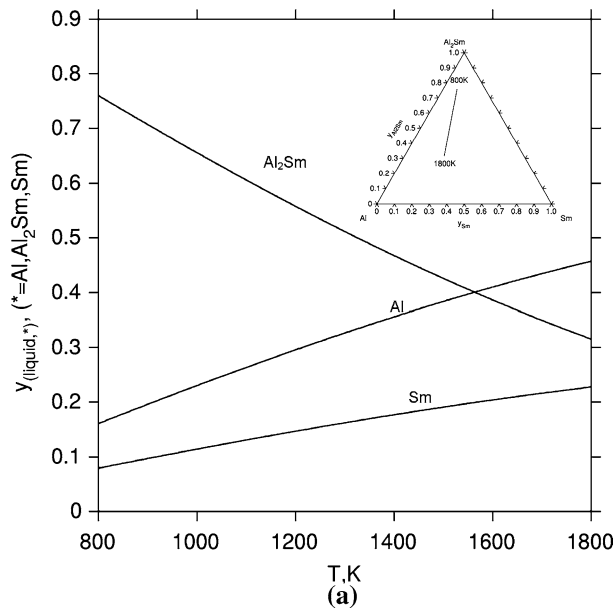


Fig. 9—Temperature dependence of (a) the associate species fraction and (b) the excess Gibbs free energy of mixing of the liquid phase at $x_{Sm} = 0.333$.

substantial improvements over the previous model,^[20] which are highlighted subsequently.

The first improvement arises from our use of the chemical associate formulation for the liquid phase, where the Al_2Sm composition is introduced as a third “component.” The benefit of this approach is that the temperature dependence of chemical ordering in the liquid phase into specific stoichiometric units, selected here as Al_2Sm , can be described. Accordingly, our results in Figure 9(a) show how the equilibrium associate fractions vary over a range of temperature (for $x_{Sm} = 0.333$), where the equilibrium fraction of Al_2Sm increases with decreasing temperature. The corresponding excess Gibbs free energy for the liquid phase at this

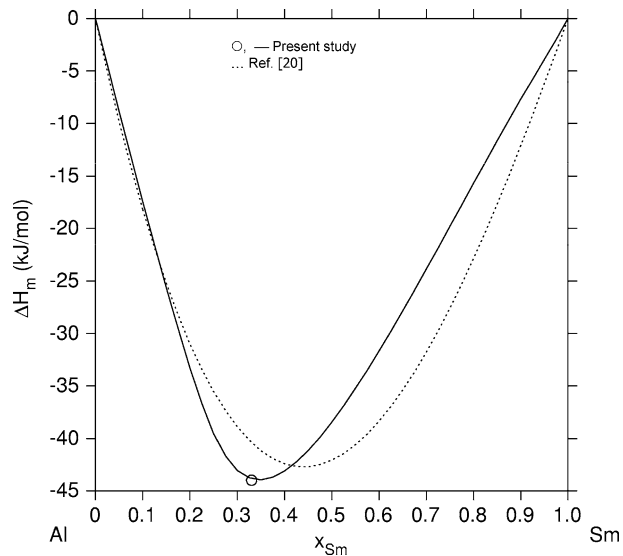


Fig. 10—Enthalpy of mixing of the liquid phase calculated at 1200 K using the parameters in Table V.

composition is plotted in Figure 9(b). The modeled enthalpy of mixing for the liquid at 1200 K is shown in Figure 10, as a function of composition, and compared with the previously reported model.^[20] Figure 10 also shows the value of ΔH_{mixing}^{liq} at 1200 K for $x_{Sm} = 0.333$, obtained from the comparison with the laves phase (Figure 7), which is used for parameter evaluation.

As a result of our treatment of the liquid phase, we arrive at a more consistent model with regard to the various phase equilibria involving the liquid phase. Our model yields a eutectic ($L \rightarrow \beta + \sigma$) temperature of 1585 K, where the previously reported model gives 1643.5 K, a value almost equal to the congruent melting temperature of 1644.9 K for the Al_4Sm - β phase.^[20] Indeed, we note a generally better agreement with experimental reports of both congruent and incongruent melting temperatures (Figure 8 and Table I).

The second improvement is attributed to our treatment of the metastable α ($Al_{11}Sm_3$) and γ (Al_4Sm) phases. In the previously reported approach, the α phase is treated as a stable phase. To be consistent with our experimental observations, however, we treat the α phase as a metastable compound with no temperature range of full stability. Figure 11(a) shows the metastable phase diagram associated with suppression of the δ phase. This is consistent with our prior work, where we have clearly mapped out the relative stability of these and other $Al_{11}Sm_3$ (or Al_4Sm) phases with respect to the liquid and relevant two-phase mixtures.

Finally, we offer one example illustrating the value of these improvements. In Figure 11(b), experimental reports^[9,10] of crystallization behavior are compared to our model description of the metastable liquidus curves for the fcc and β phases. The plotted data indicate the crystalline phases observed upon devitrification, from amorphous Al-Sm alloys of three different compositions ($x_{Sm} = 0.08, 0.10, \text{ and } 0.14$) at temperatures near

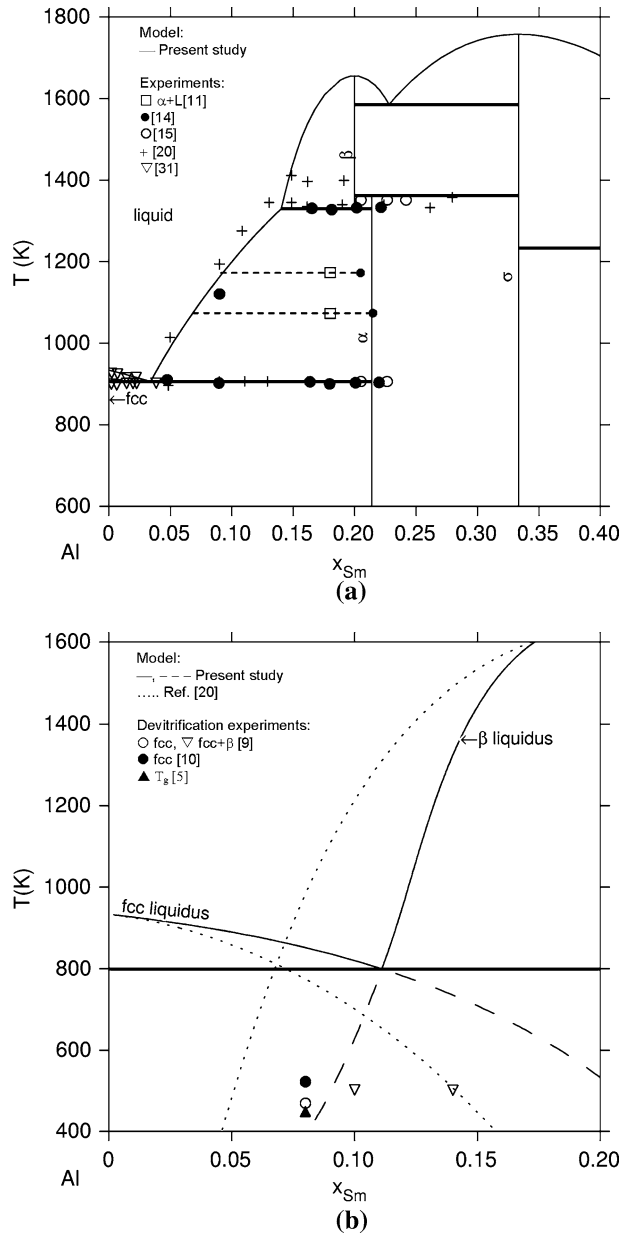


Fig. 11—Metastable Al-Sm phase diagram resulting from (a) suppression of the δ phase and (b) considering only the liquid, fcc, and $\text{Al}_4\text{Sm}-\beta$ phases, both computed using the parameters listed in Tables III and V. The tie-lines shown for the open squares in (a) indicate the metastable α phase compositions measured for short-term heat treatments (<20 h). Longer heat treatments give the $L + \delta$ equilibrium, as shown in Fig. 8.

500 K. Here it is seen that the fcc phase alone is observed for $x_{\text{Sm}} = 0.08$,^[9,10] but that both fcc and β phases are observed for $x_{\text{Sm}} = 0.10$ ^[9] and $x_{\text{Sm}} = 0.14$.^[9] We also note that, for $x_{\text{Sm}} = 0.08$, T_g has been observed to be 445 K,^[5] suggesting that the appearance of the crystalline phases at higher temperatures involves nucleation from the undercooled liquid rather than from the glass phase. Comparing these experimental reports to the results from our modeling treatment, Figure 11(b) shows that the observations are consistent with the (metastable) liquidus curves plotted for the fcc and β

phases. For $x_{\text{Sm}} = 0.08$, there is a positive driving force only for the formation of fcc. For the higher compositions, however, the temperature of 500 K lies below both fcc and β liquidus curves, and indeed, both phases are observed to form. For comparison, these same liquidus curves are shown, as modeled in Reference 20.

IV. SUMMARY AND CONCLUSIONS

By combining a solution thermodynamics approach, experimental methods, and empirical methods for evaluation of coefficients, the Gibbs free energies for all relevant phases in the binary Al-Sm system were estimated, and the associated phase equilibria are reported here. The computed phase diagram exhibits several key differences from previously reported phase diagrams. Most notably, our results include (1) stability of the $\text{Al}_4\text{Sm}-\beta$ phase from its congruent melting temperature of 1655 K to a decomposition temperature of 1333.3 K, (2) Gibbs free energy functions for the metastable $\text{Al}_{11}\text{Sm}_3-\alpha$ and $\text{Al}_4\text{Sm}-\gamma$ phases, (3) prediction of chemical ordering as a function of temperature in the liquid phase, and (4) liquidus boundaries for both stable and metastable phases that offer generally better agreement with experimental observation than previously reported phase diagrams and predictive capability regarding crystallization from an undercooled melt or amorphous solid.

ACKNOWLEDGMENTS

This work was performed within the Ames Laboratory Materials and Engineering Physics Program and was supported from the Office of Basic Energy Science, Division of Materials Science, United States Department of Energy (Contract No. W7405-Eng-82). The authors also thank Drs. A. Kracher and F.C. Laabs for assistance with EPMA and OIM measurements.

APPENDIX

The Gibbs free energy functions from Ref. [35], listed in Table III, do not include any data for ${}^\circ G_{\text{Al}}^{\text{rho}}$ and ${}^\circ G_{\text{Sm}}^{\text{fcc}}$. In this article, it is assumed that these nonstandard reference free energies can be described simply as ${}^\circ G_{\text{Al}}^{\text{rho}} = a_0^{\text{rho}} + {}^\circ G_{\text{Al}}^{\text{fcc}}$ and ${}^\circ G_{\text{Sm}}^{\text{fcc}} = a_0^{\text{fcc}} + {}^\circ G_{\text{Sm}}^{\text{rho}}$, where the parameter a_0 is determined with first-principles calculations. For this, the Vienna *ab initio* simulation package (VASP)^[40] implementation of the plane wave method is used with the Vanderbilt ultrasoft pseudopotential^[41] and a generalized gradient approximation.^[42] The Monkhost $12 \times 12 \times 12$ k points were employed for high precision. To ensure that the unit cell corresponds to a related structure, the cell shape and the internal atomic coordinates of the Al(fcc) and Sm(rho) phases were fully relaxed, while only the cell volume was relaxed for the Al(rho) and Sm(fcc) phases. The parameter a_0 is calculated as the energy difference between the fcc and rho structures, *i.e.*, $a_0^{\text{rho}} = E_{\text{Al}}^{\text{rho}} - E_{\text{Al}}^{\text{fcc}}$

(= 2283.5 J/mol) and $a_0^{\text{fcc}} = E_{\text{Sm}}^{\text{fcc}} - E_{\text{Sm}}^{\text{tho}}$ (= 890 J/mol), where E_i^{ϕ} are the computed zero-Kelvin energies for Al or Sm in the indicated structure.

REFERENCES

1. M.X. Quan, P. Haldar, J. Werth, and B.C. Giessen: *Rapidly Solidified Alloys and Their Mechanical and Magnetic Properties*, Materials Research Society, Boston, MA, 1985, vols. 2–4, pp. 299–304.
2. A. Inoue, T. Zhang, K. Kita, and T. Masumoto: *Mater. Trans., JIM*, 1989, vol. 30, pp. 870–77.
3. A. Inoue: *Progr. Mater. Sci.*, 1998, vol. 43, pp. 365–520.
4. G. Wilde, H. Sieber, and J.H. Perepezko: *J. Non-Cryst. Solids*, 1999, vol. 252, pp. 621–25.
5. G. Wilde, H. Sieber, and J.H. Perepezko: *Scripta Mater.*, 1999, vol. 40, pp. 779–83.
6. S.C. Tjong and J.Q. Wang: *Z. Metallkd.*, 2001, vol. 92, pp. 610–16.
7. J.H. Perepezko, R.J. Hebert, and W.S. Tong: *Intermetallics*, 2002, vol. 10, pp. 1079–88.
8. J.H. Perepezko, R.J. Hebert, R.I. Wu, and G. Wilde: *J. Non-Cryst. Solids*, 2003, vol. 317, pp. 52–61.
9. J.Q. Guo, K. Ohtera, K. Kita, J. Nagahora, and N.S. Kazama: *Mater. Lett.*, 1995, vol. 24, pp. 133–38.
10. P. Rizzi, M. Baricco, S. Barace, and L. Battezzati: *Mater. Sci. Eng., A*, 2001, vols. 304–306, pp. 574–78.
11. S.H. Zhou and R.E. Napolitano: *Metall. Mater. Trans. A*, 2007, vol. 38A, pp. 1145–51.
12. A. Iandelli: *The Physical Chemistry of Metallic Solutions and Intermetallic Compounds*, National Physical Laboratory, Teddington, Great Britain, Her Majesty's Stationery Office, London, 1959, vol. I, pp. 3F1–10.
13. H.J. Wernick and S. Geller: *Trans. TMS-AIME*, 1960, vol. 218, pp. 866–68.
14. K.H.J. Buschow and J.H.N. van Vucht: *Philips Res. Rep.*, 1965, vol. 20, pp. 15–22.
15. F. Casteels: *J. Less-Common Met.*, 1967, vol. 12, pp. 210–20.
16. D.E. Mesquita, A.H. Gomes, and K.H.J. Buschow: *Acta Crystallogr.*, 1967, vol. 22, pp. 497–501.
17. K.H.J. Buschow and J.H.N. van Vucht: *Philips Res. Rep.*, 1967, vol. 22, pp. 233–45.
18. K.A.J. Gschneidner and F.W. Calderwood: *Bull. Alloy Phase Diagrams*, 1989, vol. 10, pp. 37–39.
19. T.B. Massalski: *Binary Alloy Phase Diagrams*, ASM International, Materials Park, OH, 1990, pp. 213–14.
20. A. Saccone, G. Cacciamani, D. Maccio, G. Borzone, and R. Ferro: *Intermetallics*, 1998, vol. 6, pp. 201–15.
21. F. Sommer, M. Keita, H.G. Krull, B. Predel, and J.J. Lee: *J. Less-Common Met.*, 1988, vol. 137, pp. 267–75.
22. C. Colinet, A. Pastural, and K.H.J. Buschow: *J. Chem. Thermodyn.*, 1985, vol. 17, pp. 1133–39.
23. G. Borzone, A.M. Cardinale, A. Saccone, and R. Ferro: *J. Alloys Compd.*, 1995, vol. 220, pp. 122–25.
24. G. Borzone, A.M. Cardinale, N. Parodi, and G. Cacciamani: *J. Alloys Compd.*, 1997, vol. 247, pp. 141–47.
25. W.G. Jung, O.J. Kleppa, and L. Topor: *J. Alloys Compd.*, 1991, vol. 176, pp. 309–18.
26. G. Cacciamani and R. Ferro: *CALPHAD*, 2001, vol. 25, pp. 583–97.
27. Y.U.O. Esin, S.P. Kolesnikov, V.M. Baev, M.S. Petrushevskii, and P.V. Gel'd: *Russ. J. Phys. Chem.*, 1981, vol. 55, pp. 893–94.
28. F. Sommer and M. Keita: *J. Less-Common Met.*, 1987, vol. 136, pp. 95–99.
29. G. Borzone, G. Cacciamani, and R. Ferro: *Metall. Mater. Trans. A*, 1991, vol. 22A, pp. 2119–23.
30. G.N. Zviadadze, L.A. Chkhikvadze, and M.V. Kereselidze: *Soobshch. Akad. Nauk Gruz. SSR*, 1976, vol. 81, pp. 149–52.
31. V.I. Kononenko and S.V. Golubev: *Izv. Akad. Nauk SSSR, Met.*, 1990, vol. 2, pp. 197–99.
32. Y.U.O. Esin, G.M. Ryss, and P.V. Gel'd: *Z. Fiz. Khim.*, 1979, vol. 53, pp. 2380–81.
33. G. Borzone, A.M. Cardinale, G. Cacciamani, and R. Ferro: *Z. Metallkd.*, 1993, vol. 84, pp. 635–40.
34. Test materials were supplied by the Materials Preparation Center, Ames Laboratory, US DOE, Basic Energy Sciences, Ames, IA (www.mpc.ameslab.gov).
35. A.T. Dinsdale: *CALPHAD*, 1991, vol. 4, pp. 317–425.
36. O. Redlich and A.T. Kister: *Ind. Eng. Chem.*, 1948, vol. 40, pp. 345–48.
37. F. Sommer: *Z. Metallkd.*, 1982, vol. 73, pp. 72–86.
38. H.G. Krull, R.N. Singh, and F. Sommer: *Z. Metallkd.*, 2000, vol. 91, pp. 356–65.
39. S.H. Zhou and R.E. Napolitano: *Acta Mater.*, 2006, vol. 54, pp. 831–40.
40. J.P. Perdew, J.A. Chevary, S.H. Vosko, K.A. Jackson, M.R. Pederson, D.J. Singh, and C. Fiolhais: *Phys. Rev. B*, 1992, vol. 46, pp. 6671–87.
41. D. Vanderbilt: *Phys. Rev. B*, 1990, vol. 41, pp. 7892–95.
42. G. Kresse and D. Joubert: *Phys. Rev. B*, 1999, vol. 59, pp. 1758–75.